Tectonophysics 918 (2026) 230979

Contents lists available at ScienceDirect

Tectonophysics

journal homepage: www.elsevier.com/locate/tecto

A quantitative reassessment of the 1934 Bihar-Nepal earthquake and its seismotectonic implications☆

Laurent Bollinger [a,*], Emile A. Okal [b]

[a] CEA, DAM, DIF, F-91297 Arpajon, France
[b] Department of Earth and Planetary Sciences, Northwestern University, Evanston, IL 60208, USA

ARTICLE INFO

Keywords:
1934 Bihar-Nepal earthquake
Seismic moment
Main Himalayan Thrust
Rupture scenario
Scaling laws

ABSTRACT

The 1934 Bihar-Nepal earthquake is the largest instrumental earthquake to strike Nepal. However, its moment magnitude is still associated with considerable uncertainty in the literature, with a wide range of values between 8.0 ± 0.3 and as high as 8.4. In this paper we re-evaluate its seismic moment using teleseismic surface wave records from 6 stations. A total of 10 independent measurements lead to a seismic moment of 3.8×10^{21} N.m ($M_w = 8.3 \pm 0.1$), releasing more than 4 times the seismic moment of the 2015 Gorkha earthquake.

Given this seismic moment release, we consider several rupture scenarios with different length-width-slip estimates for the mainshock. We compare them with slip estimates derived from field observations and show that the average slip is likely to have been between 8 and 16 m, a value significantly larger than previous estimates. We compare the dimensions obtained with those of other intercontinental thrust earthquakes. The results reduce the uncertainties associated with the assessment of the deficit of the seismic moment accumulated since the great earthquakes of the medieval period in Nepal.

1. Introduction

The purpose of this paper is the reassessment of the long-period size, expressed as its seismic moment M_0, of the great Nepal-Bihar earthquake of 15 January 1934. We are motivated by the recent occurrence of the Gorkha, Nepal earthquake of 25 April 2015 ($M_w = 7.9$), which ruptured a contiguous segment of the Himalaya Main Thrust to the West. In this context, a quantified comparison of the events of 1934 and 2015 is an important step in assessing the seismic hazard in that region, affected since medieval times by several well documented earthquakes (e.g. Pant, 2002; Bollinger et al., 2016). The 2015 rupture propagated almost unilaterally along a 140 to 160-km long segment of the main Himalayan thrust fault, from a 17-km deep hypocenter located at the brittle-ductile transition, under the foot of the high Himalaya barrier, and accommodated an average coseismic slip of ~4 m (e.g., Avouac et al., 2015; Grandin et al., 2015). To the East, the rupture abutted on the supposed western edge of the inferred subsurface rupture of the great Bihar-Nepal earthquake of 15 January 1934 ($M \geq 8$) (Adhikari et al., 2015; Bilham, 2019). However, the latter's rupture broke the surface in eastern Nepal (Sapkota et al., 2013; Bollinger et al., 2014; Rizza et al., 2019; Riesner et al., 2023), while the 2015 rupture stopped halfway between the front of the high range and the most frontal thrusts. Besides local cracks as well as suspected rupture of secondary faults in the hanging wall, as well as several landslides, the 2015 earthquake left no signature along the updip-end of the Main Himalayan thrust fault system. Therefore it offers few or no direct constraints on estimates of the reach of paleoseismic earthquakes in eastern Nepal. While they dominate the seismic moment release (Stevens and Avouac, 2016; Bollinger et al., 2016) such rare events are seldom documented by more than a few morpho-sedimentological records along the main frontal thrust.

Thanks to the explosion in digital instrumentation over the past few decades, the 2015 event stands as the best studied of all Himalayan earthquakes and contributes a significant part of our knowledge of large inter-continental earthquakes generated on mega-thrust systems. In particular, its moment was inverted as part of the standardized GlobalCMT project (Dziewonski et al., 1981; Ekström et al., 2012) as $M_0 = 8.7 \times 10^{20}$ N.m, equivalent to $M_w = 7.9$ (Kanamori, 1977). The earthquake also features a slowness parameter $\Theta = -5.21$ (Newman and Okal, 1998), characteristic of most low-angle shallow thrust events; the strong accelerations responsible for the considerable destruction can be

☆ This article is part of a Special issue entitled: 'Paul Tapponnier' published in Tectonophysics.

* Corresponding author.
E-mail address: laurent.bollinger@cea.fr (L. Bollinger).

https://doi.org/10.1016/j.tecto.2025.230979
Received 9 July 2025; Received in revised form 29 October 2025; Accepted 30 October 2025
Available online 1 November 2025

attributed to the presence of a thick sedimentary layer in the Kathmandu Valley (e.g. Bijukchchen et al., 2017), rather than a source spectrum blue-shifted towards higher frequencies.

By contrast, the historical 1934 Bihar-Nepal earthquake predates the development of modern seismological instrumentation and its analysis has suffered from the general scarcity of records available for use in modern algorithms (Okal, 2015). In particular, and as detailed below, published estimates of its seismic moment vary by a factor of ~6, making it difficult to obtain a meaningful comparison with the more recent 2015 event. Estimates of conventional magnitudes, obtained either by traditional seismological techniques (Gutenberg and Richter, 1954; Richter, 1958) or converted from estimates of macroseismic intensities (Ambraseys and Douglas, 2004; Szeliga et al., 2010) also vary widely, from M = 8.0 to 8.4.

Given available constraints on fault length along strike, and on the downdip extent of the rupture, an uncertainty of a factor of 6 in moment (0.5 units of M_w) could lead to differences of a factor close to 4 in mean coseismic slip, and hence in return time between end member models of its seismic source. Nevertheless, the ample surface rupturing of the 1934 Bihar-Nepal earthquake has made this event a fundamental reference for studies of large Himalayan earthquakes by geomorphologists and paleoseismologists.

In this general context, these remarks warrant a better resolution of the seismic moment of the 1934 earthquake, to better constrain the seismogenic potential of the local thrust system, and more generally the regional seismic hazard.

This paper provides a modern reassessment of the 1934 Bihar-Nepal earthquake, most importantly of its seismic moment. We review both epicentral locations and magnitudes available in the literature, and provide new estimates based on modern algorithms. Using a set of 10 teleseismic surface wave records at six sites worldwide, we obtain a value of $M_0 = 3.8 \times 10^{21}$ N.m equivalent to $M_w = 8.3$, on the upper bound of previously published values. Finally, we discuss the implications of this new quantitative constraint on alternative scenario of

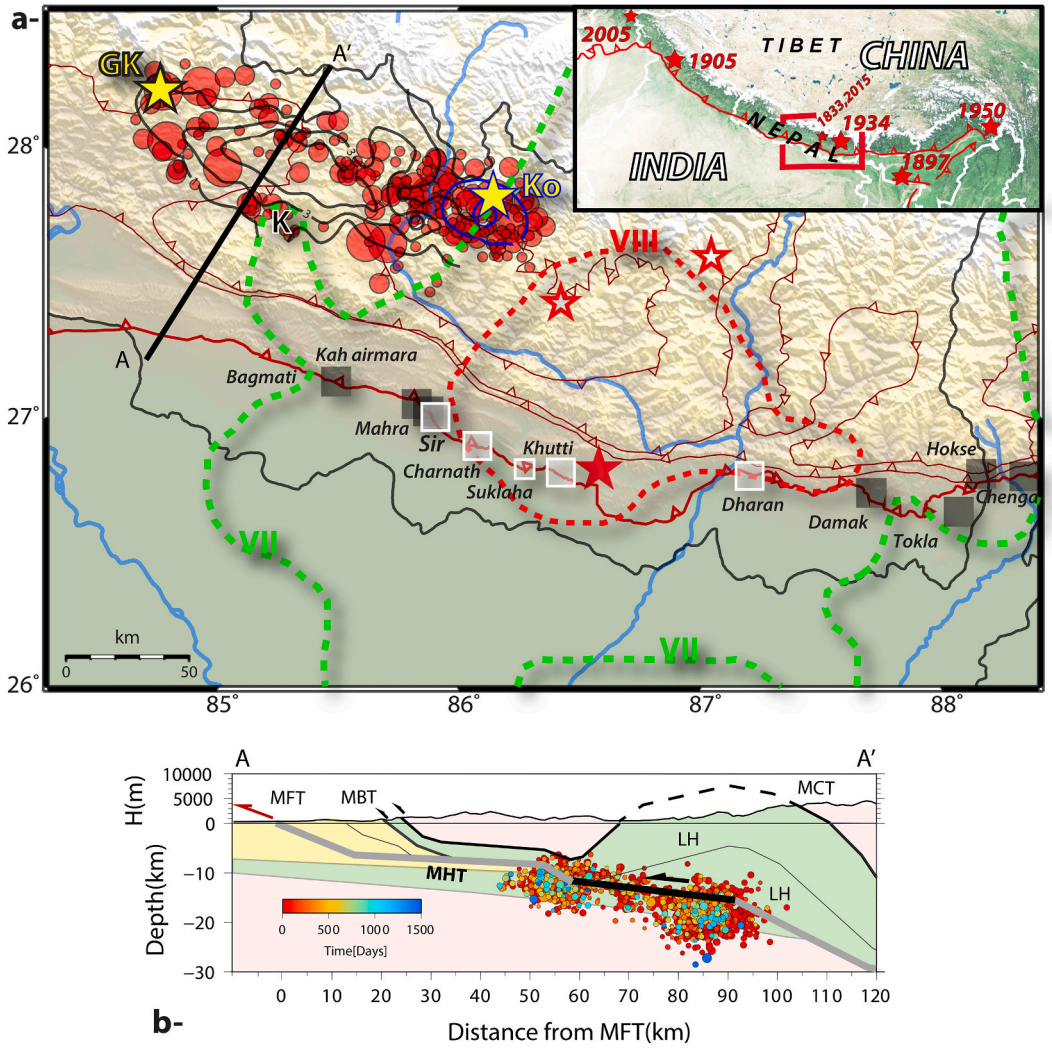

Fig. 1. (a): Map of the epicentral area of the 1934 and 2015 earthquakes. The yellow stars are the 2015 Gorkha (Gk) and Kodari (Ko) earthquakes epicenters, and the red dots their aftershocks (M ≥ 4, after Adhikari et al., 2015). The large red star is our relocated solution for 1934 (see Fig. 2 and text for details) while the open red stars with white and grey filling correspond to Chen and Molnar's (1977) epicenter and Martin and Szeliga (2010) macroseismic epicenter. The dotted lines show the 1934 isoseismals MMI VII (green) and VIII (red), after Sapkota et al. (2016). K stands for Kathmandu. Black and blue contours are respectively slip contours of the Gorkha and Kodari earthquakes, with isocontours every meter.White and grey squares are paleoseismological trenches and morphotectonic sites with dated ruptures (Sapkota, 2011; Sapkota et al., 2013; Bollinger et al., 2014; Bernard et al., 2018; Rizza et al., 2019; Wesnousky et al., 2017a, 2017b, 2019; Riesner et al., 2023; Brice et al., 2024). White squares are sites with relevance to the 1934 earthquake (see main text). Lines with small chevrons indicate, from south to north, the Main Frontal, Main Boundary and Main Central thrusts. Inset shows the location of the largest Himalayan earthquakes. (b): cross section of the 2015 epicentral area along profile AA'. Aftershocks from Adhikari et al. (2023) are colour-coded according to their date of occurrence following the main shock. (For interpretation of the references to colour in this figure legend, the reader is referred to the web version of this article.)

coseismic slip distribution and compare the 1934 event's parameters with those of other thrust earthquakes used to calibrate empirical relations between earthquake parameters.

2. The January 15th 1934 Bihar earthquake

2.1. General description and macroseismic location

In the general framework of Fig. 1, the 1934 earthquake devastated a large region of Eastern Nepal and Northern India (Bihar state), affecting millions of households, with a death toll estimated between 7200 and more than 20,000 in India, and 8500 in Nepal (Rana, 1935; Roy, 1939; Marcussen, 2023). Three distinct regions were severely affected: (1) the Kathmandu valley, (2) a large region in eastern Nepal and (3) the north and central Bihar state in India. In the latter, the Geological Survey of India mapped widespread sand vents, liquefaction and in a more general way spectacular damages along a 300 km-long region north of the Ganga river. This area was named the " Slump belt" following the mapping of intense soil liquefaction and slumping. These effects were accompanied by a regional subsidence of tens of centimeters measured by comparison with benchmark leveling (Bomford, 1937; Bilham et al., 1998). Further North, the eastern districts of Nepal were strongly affected, in particular the Siwaliks fold and thrust belt as well as the lesser Himalayas, where numerous landslides were reported. Despite the rural environement, the fatality rates in these regions exceeded 0.1 % (Sapkota et al., 2016). Higher fatality rates were only reported in the Kathmandu valley, where they exceeded 5 % in the most urban areas due to high building vulnerability (Sapkota et al., 2016), and probably by analogy with the 2015 event, site response in the presence of thick sedimentary layering.

Because the most severe damages probably reflected strong vulnerability of soils and buildings to seismic waves as well as a short distance to the seismic source, the three regions mentioned above were used by early investigators as epicentral estimates. Rana (1935) first proposed a macroseismic epicenter in Nepal, under the Lesser Himalayas, based on locally strong damage and catastrophic testimonies. Later, Dunn et al. (1939) proposed a source in India, within the slump belt, again on account of locally strong damage. However, the high macroseismic intensities reported in the slump belt appear to be mainly related to liquefaction and sediment slumping, and could therefore bias the location of macroseismic epicentral estimates to the south (Bilham et al., 1998; Ambraseys and Douglas, 2004; Hough and Bilham, 2008).

2.2. Instrumental relocations

As in the case of macroseismic estimates, there is considerable scatter among epicenters of the 1934 earthquake proposed by various authors based on instrumental relocations, as summarized on Fig. 2. The earliest epicenter was given by Roy (1939) at 26.3°N, 86.3°E, within the slump belt (yellow circle on Fig. 2), with a focal depth of 14.8 km (and origin time 8:43:21 GMT). Later estimates include the ISS original location (light blue triangle at 26.6°N, 86.8°E) and Gutenberg and Richter (1954) solution (green inverted triangle at 26.5°N, 86.5°E). The USGS catalog lists the event more than 100 km to the Southwest, at 26°N, 85.5°E (yellow diamond).

Modern relocations include Engdahl et al.'s (1998), part of their Centennial catalog (brown square at 26.77°N, 86.76°E) and the latest ISC relocation, generally regarded as authoritative, at 26.88°N, 86.59°E (dark blue triangle), but appear unlikely based on modern. Finally, a probably more correct modern estimate is Chen and Molnar's (1977), offset about 100 km to the North, at 27.55°N, 87.09°E (white circle on Fig. 2, and associated by the authors with an uncertainty of ±12.5 km), a location interpreted by Molnar and Qidong (1984) as the down-dip end of the locked Main Himalayan Thrust fault zone. The origin of that solution remains unclear, even though it would be supported by the observation that Himalayan earthquakes generally nucleate at the downdip end of the locked faut zone, estimated to reside below the top

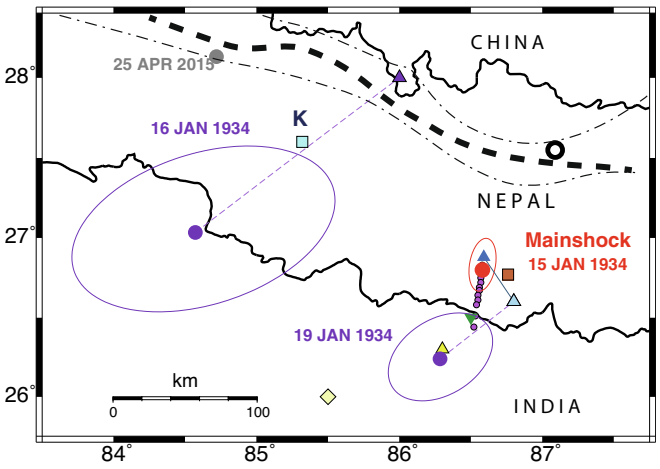

Fig. 2. Relocation of the 1934 Bihar-Nepal earthquake. Our relocation is shown as the solid red dot, with associated Monte Carlo ellipse. The original ISS location is shown as the light blue triangle, and the modern ISC relocation based on the same dataset as the dark blue triangle. Other solutions are those of Gutenberg and Richter (1954) (green inverted triangle), Roy (1939) (yellow triangle), the USGS (yellow diamond), Engdahl et al. (1998) (brown square) and Chen and Molnar (1977) (white circle). Also shown are original ISS epicenters (purple triangles) and our relocations (purple triangles with associated Monte Carlo ellipses) for the two main aftershocks of 16 and 19 January 1934, as well as the ISC location of the 2015 Gorkha earthquake (grey circle). The small magenta dots illustrate the moveout of the epicenters of constrained-depth relocations. Finally, the city of Kathmandu is shown as the light blue square (and the letter "K"). The bold black dashed line shows the downdip edge of the midcrustal ramp inferred from surface geology (Hubbard et al., 2016) and the thin dot-dashed line the modeled downdip limit of coupling across Nepal from Lindsey et al. (2018). (For interpretation of the references to colour in this figure legend, the reader is referred to the web version of this article.)

of the high Himalayan range (Ader et al., 2012; Lindsey et al., 2018).

We conducted our own relocation of the 1934 epicenter based on 244 P and S arrival times listed in the ISC Bulletin, using the interactive iterative algorithm of Wysession et al. (1991), which provides a 95 % confidence ellipse, obtained through a Monte Carlo procedure injecting Gaussian noise into the dataset. For an earthquake in the early 1930s, we use a standard deviation $\sigma_G = 5$ s for the noise. The solution (26.80°N, 86.58°E) features a remarkably small ellipse of confidence, which contains the modern ISC relocation. The dataset cannot resolve hypocentral depth, with floating depth relocations failing to converge. Following Rees and Okal (1987), we examine on Fig. 3 the variation of the r.m.s of time residuals in constrained depth relocations. They are found to increase monotonically with hypocentral depth, but the precision of the times listed in the original ISS bulletins (1 s) cannot resolve a minimum above a depth of ~50 km. In addition, Fig. 3 shows that the moveout of those relocated epicenters takes place in a SSW direction, opposite the trend of subduction of the Indian plate, as also confirmed by the cross-section of Fig. 3, all these arguments supporting a shallow source. We also note that the modern ISC relocation similarly uses a constrained depth of 15 km, while the depth of the 2015 Gorkha event was inverted to 13 km. Note also that depth phases pP have been reported in the ISC bulletin at GTT and KEW, 6 s and 5 s after the direct P arrival, at epicentral distances of 60° and 67°, respectively. Considering that the 1 s difference likely reflects uncertainties in picking, taking an average 5.5 +/− 0.5 s for a velocity Vp ~ 6.0 +/− 0.2 km.s^{-1} yields a depth of 17 +/− 3 km below topography. If these arrivals indeed correspond to pP phases – and not to the direct P of eventual subsources of the large rupture - the hypocentre is shallow whatever reasonable parameters are used. We also relocated the two main aftershocks of 16 and 19 January, for which arrival times are listed in the ISS, but which were not relocated in the modern ISC catalog. While their Monte Carlo ellipses are much larger on account of their smaller size, and hence smaller dataset of

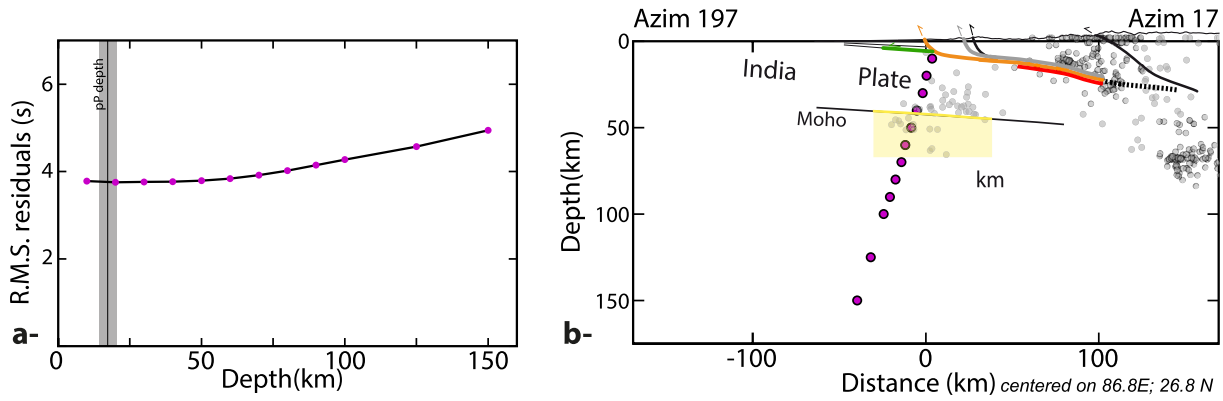

Fig. 3. Left: Root-mean-squares residuals of travel times for constrained-depth relocations of the great 1934 earthquake, as a function of the constrained depth. Note the monotonic increase with depth, but the absence of resolution of a minimum for h ≤ 50 km. The best depth derived from the pP depth phase picks available in ISC bulletin is represented by the vertical black line and its uncertainty by the grey band (see text for assumptions and limits). Right: Cross of hypocenters from constrained-depth relocations (magenta dots) superimposed on background seismicity (local catalog from Monsalve et al., 2006: grey dots) and the main geological structures (See legend Fig. 1b in Bollinger et al., 2014). (For interpretation of the references to colour in this figure legend, the reader is referred to the web version of this article.)

arrival times, the preferred epicenters are separated by 180 ± 60 km, and they could represent the extremities of the coseismic rupture of the 1934 event. The mainshock and aftershocks determined with our methodology fall surprisingly several dozens of kilometers south of the downdip limit of coupling of the thrust, where the Gorkha earthquake nucleated. We get what we get in term of epicentral determination, but we recognize that the epicenter is not optimally constrained. This epicenter differs from the relocation of Chen and Molnar (1977), which is more consistent with recent knowledge of the behavior of the main Himalayan Thrust, with a north-south strain gradient below the High Range, rather than below the Siwalik Hills (See location of the mid-crustal ramp and downdip end of the locked fault zone in Fig. 2).

In this context, the scatter between the various macroseismic and instrumental locations led to an initial absence of consensus on the rupture scenario of the 1934 earthquake. In particular, the identification of a medieval surface rupture along the MFT in central Eastern Nepal (Lavé et al., 2005) suggested that by contrast, the 1934 event had been blind, i.e., too small to rupture the surface.

However, recent work has finally identified its surface rupture in Southcentral Nepal, along the trace of the Main Frontal Thrust (Sapkota et al., 2013), in the mesoseismal area at Sir Khola (Sapkota et al., 2013; Bollinger et al., 2014), later at Charnath Khola (Rizza et al., 2019) and finally at Khutti Khola (Riesner et al., 2023) (see Fig. 1).

3. Size of the 1934 earthquake

3.1. Early magnitude estimates

Because the 1934 Bihar-Nepal earthquake predates the introduction of the concept of magnitude by Richter (1935), early investigators merely offered qualitative comparisons of its size relative to the 1833 event, the only prior large earthquake documented significantly in Nepal (Rana, 1935; Dunn et al., 1939; Bilham, 1995). Similar comparisons were also provided with other great instrumentally recorded Indian earthquakes, such as the 1905 Kangra event, or even the 1897 earthquake under the Shillong plateau (e.g. Subedi and Hetényi, 2021).

As part of their monumental compilation "Seismicity of the Earth", Gutenberg and Richter (1941) assigned the event a magnitude $M_{GR} = 8$ ¼, later transcribed as 8.3 in further editions (Gutenberg and Richter, 1949, 1954). Such values are generally considered comparable to present-day 20-s M_s (Geller and Kanamori, 1977), as defined by the Prague formula (Vaněk et al., 1962). Richter (1958) proposed a value of M = 8.4 as "unified" magnitude, a scale often found to overestimate the more widely used M_s. The M_{GR} estimate was later included in Abe's (1981, 1984) catalogs, as well as an independently measured body-wave magnitude $m_B = 7.8$, this large value (for a body-wave magnitude) being obtained at a period of 10 s, for which the standard algorithm proposed by Gutenberg and Richter (1956) and enshrined by Vaněk et al., 1962 into the present-day short-period m_b scale may not be valid (Saloor and Okal, 2020). The revised ISC catalog features a reassessment of M_s as 8.2 ± 0.2 based on 7 original station reports. A similar approach by Ambraseys and Douglas (2004) yielded the essentially equivalent value $M_s = 8.15 \pm 0.3$ from a substantially larger dataset. An additional estimate of classical magnitude is given as 8.4 by Båth and Duda (1979), presumably using surface waves.

The apparent discrepancy of reported magnitudes (from 8.1 to 8.4) illustrates subtle differences in early algorithms used by various authors, as well as the general lack of reliability of M_s for very large earthquakes, as the scale saturates around 8.2 (Kanamori and Anderson, 1975; Geller, 1976) due to source finiteness effects (Ben-Menahem, 1961).

3.2. Previous moments estimates

More reliable of course is the physical measurement of a seismic moment, taken at traditionally much longer periods, thus avoiding destructive interference due to finiteness. For the 1934 earthquake, a reference study is Chen and Molnar's (1977) who used a set of six historical records of Love and Rayleigh waves at intermediate periods (50 to 100 s), to obtain a value of $M_0 = 1.1 \times 10^{21}$ N.m, equivalent to $M_w = 8.0$, and only slightly larger than for the 2015 Gorkha event. By contrast, Singh and Gupta (1980) later proposed a value four times larger ($M_0 = 4.4 \times 10^{21}$ N.m, equivalent to $M_w = 8.4$), with their dataset significantly scattered between values of 1.3 and 9.5 × 10 ^{21} N.m, equivalent to a spread of ~0.6 units of M_w, a discrepancy possibly.

In addition, we note that Brune and King (1967) and Brune and Engen (1969) proposed a "Mantle magnitude" $M_M = 8.0$ for the 1934 earthquake, based on the spectral amplitudes of Rayleigh and Love waves at 100 s. While their approach clearly seeks to avoid the saturation of shorter-period scales due to source finiteness, these authors do not provide a direct link between M_M and seismic moment M_0.

In their study, Chen and Molnar (1977) used a thrust focal mechanism on a fault dipping 20° under the Himalayas, to compute their estimate (1.1 × 10^{21} N.m). However, Molnar and Qidong (1984) later argued that the examination of recent lower-level seismicity along the Main Himalayan Thrust suggests a shallower dip, which they take as 5°, which in turn would result in a larger seismic moment, namely 4.1 × 10^{21} N.m, given the classical trade-off between these dip and M_0 for shallow-angle pure thrust mechanisms (Tsai et al., 2011).

A further discrepancy between the studies of Chen and Molnar (1977) and Molnar and Qidong (1984) comes from the widely different fault dimensions that they assign to the source: 130 km × 50 km for the former, vs. 200 km x 120 km for the latter, these numbers being enough to reconcile the differents values of the moment with strikingly similar values of the average seismic slip: 5.4 m for Chen and Molnar's (1977) vs. 4.7 m for Molnar and Qidong (1984), using a crustal rigidity of 3.2×10^{11} dyn/cm^2. Incidentally both values are very comparable to the average slip of ~4 m proposed for the smaller 2015 Gorkha earthquake (Wang and Fialko, 2015). In the absence of a discussion of the extended fault area by Molnar and Qidong (1984), and given the scarcity of documented aftershocks, it remains difficult to resolve this discrepancy. We simply note that the GlobalCMT focal mechanism inverted for the 2015 Gorkha event (φ =287°, δ = 6°, λ = 96°) also features a very shallow dip.

We note finally that in their compilation of historical moments included as part of the ISC-GEM project, Lee and Engdahl (2015) list Chen and Molnar's (1977) lower value (equivalent to $M_w = 8.0$), albeit with the caveat of a relatively poor quality factor ("C+") due to large uncertainties.

3.3. Reassessment of the seismic moment

In this section, we conduct an independent reassessment of the seismic moment of the 1934 earthquake, based on the mantle magnitude concept (Okal and Talandier, 1989). At each station and at each frequency, the algorithm derives from the Fourier spectrum of ground motion of mantle surface waves a mantle magnitude M_c theoretically related to the seismic moment through.

$$M_c = \log_{10} M_0 – 20 \quad (1)$$

where M_0 is in dyn x cm, and after correction for focal mechanism. It was successfully applied to historical events (e.g. Okal and Borrero, 2011; Salaree and Okal, 2018).

In the present case, we were able to obtain 10 adequate waveforms (8 Love and 2 Rayleigh) at six stations listed in Table 1. Representative seismograms are shown on Figs. 4, 5 and 6. We use the focal mechanism of the 2015 Gorkha earthquake and a source depth of 15 km to compute the corrected magnitude Mc. The frequency band used (5–12 mHz) is significantly lower than in Chen and Molnar's (1977) study, thus minimizing the effect of finiteness of the source. Results are presented on Fig. 7. The average of all 49 measurements of Mc is 8.58 with a standard deviation of 0.26. This translates to $M_0 = 3.84 \times 10^{21}$ N.m, equivalent to $M_w = 8.32 \pm 0.17$. A remarkable result is the general constancy of the moment throughout the frequency band considered. A linear regression of Mc with frequency is shown as the magenta dashed line, and its parameters are listed at bottom left. Note the extremely weak slope (−0.01 logarithmic units per mHz) indicating an essentially flat spectrum. This is in contrast with events exhibiting source slowness, such as "tsunami earthquakes" whose spectrum is red-shifted with a negative slope typically larger than 0.07 units/mHz (in absolute value), as documented for

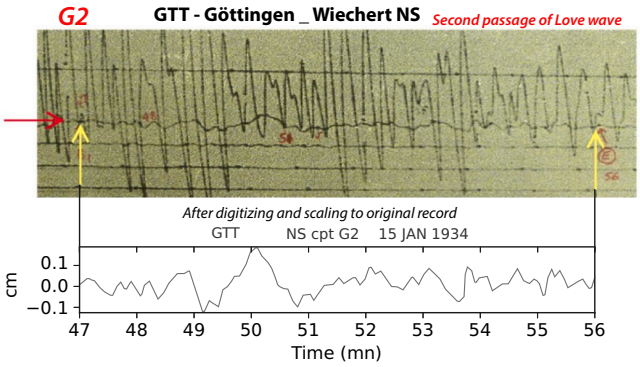

Fig. 4. Record of the second passage of the Love waves on the Wiechert at Göttingen (GTT) (at 61.4° from the epicenter), 47 min after the main shock, pointed and delimited by the red and yellow arrows. Top: original signal on the N-S component. Bottom: waveform after digitizing and scaling to original record. (For interpretation of the references to colour in this figure legend, the reader is referred to the web version of this article.)

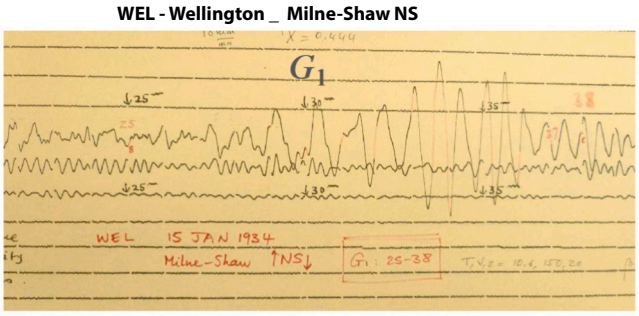

Fig. 5. Original signal recorded on the Milne-Shaw seismometer (N-S component) in Wellington (WEL), at 105.8° of the epicenter.

example in the case of the "tsunami earthquake" aftershocks of the 1923 Kamchatka and 1932 Manzanillo great earthquakes (Okal and Borrero, 2011; Salaree and Okal, 2018). In the present case, we conclude that the 1934 Bihar-Nepal earthquake does not feature such anomalous behavior, but rather has what amounts to a textbook source spectrum.

3.4. Energy-to-moment ratio and parameter Θ

In this section, we estimate an energy-to-moment ratio using the parameter.

$$\Theta = \log_{10} E^E / M_0 \quad (2)$$

where E^E is an estimate of the energy radiated into the generalized *P* wave at distances Δ between 35 and 80 degrees, in the formalism of Newman and Okal [1998], whose application to analog records of

Table 1
Seismic records used in this study.

Code	Station	Distance (°)	Azimuth (°)	Instrument	Phase	M_c	M_0 (10^{21} N.m)
DBN	*De Bilt*	*64.2*	*317*	*Galitzin*	*G3*	*8.42*	*2.6*
					G2	*8.51*	*3.3*
CTO	*Cape town*	*88.6*	*231*	*Milne-Shaw*	*G1*	*8.54*	*3.5*
HON	*Honolulu*	*101.2*	*59*	*Milne-Shaw*	*R1*	*8.18*	*1.5*
					G1	*8.69*	*5.0*
RIV	*Riverview*	*85.9*	*131*	*Wiechert*	*R1*	*8.91*	*8.0*
					G1	*8.70*	*5.0*
GTT	*Göttingen*	*61.4*	*316*	*Wiechert*	*G2*	*8.69*	*5.0*
					G1	*8.48*	*3.0*
WEL	*Wellington*	*105.8*	*128*	*Milne-Shaw*	*G1*	*8.64*	*4.4*
Seismic moment estimated from the geometric mean of all 50 M_c values							***3.8***

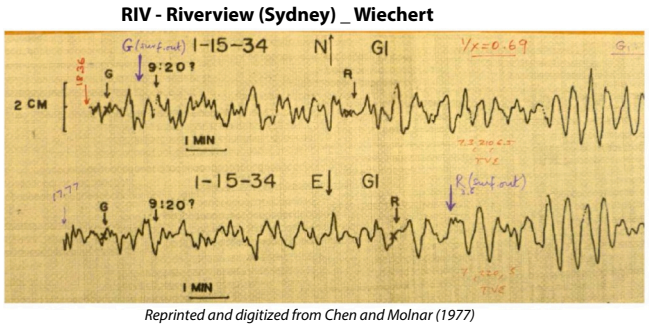

Reprinted and digitized from Chen and Molnar (1977)

Fig. 6. Waveforms of the passage of the Love waves on the Wiechert at Riverview (RIV Sydney, Australia) at 85.9° of the epicenter reprinted and digitized from Chen and Molnar (1977).

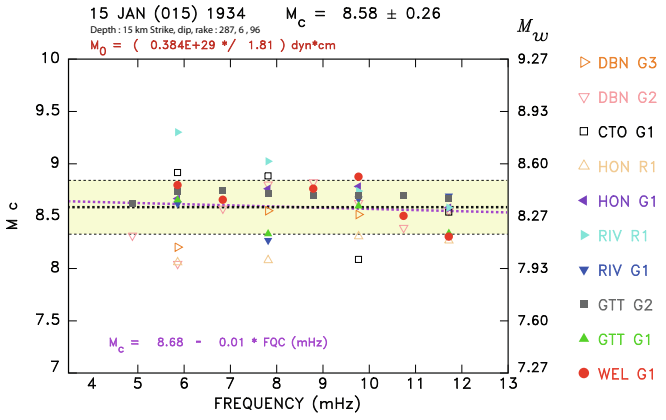

Fig. 7. Values of corrected mantle magnitude Mc (Okal and Talandier, 1989) as a function of frequency for 10 records of of mantle waves of the 1934 Bihar-Nepal earthquakes, each using a different symbol (see list at right). The equivalent M_w scale is also shown on the right. The black dashed line corresponds to the average magnitude (geometrical average of the moment values), and the magenta dashed line shows a linear regression of the dataset with frequency, as listed at bottom left. Note the extremely low value of its slope (−0.01 $\log_{10}$ units per mHz), indicating that the earthquake does not feature source slowness. The « */ 1.81 » associated to the M_0 stands for the factor of imprecision of the geometric regression. The average M_c is 8.58 ±0.26 and corresponds to a seismic moment of 0.38 × 10^{29} dyn.cm (3.8 × 10^{21} N.m) and a Mw = 8.3. (For interpretation of the references to colour in this figure legend, the reader is referred to the web version of this article.)

distant events has been validated by Okal and Kirby [2002], and subsequently applied to numerous earthquakes. It is important to note that the resulting values of Θ for historical earthquakes span the full range of Θ values obtained with modern digital data, from slow "tsunami earthquakes" [Okal and Borrero, 2011] to fast ones [Okal et al., 2016], thus ruling out the possibility of a systematic bias in the method when using analog data. We were able to process 13 records, listed in Table 2, from stations in Europe and Japan. The resulting Θ values vary from −4.54 to −3.85 with an average value.

$$< \Theta \geq -4.25 \pm 0.19 \quad (3)$$

This result is plotted as the green square bull's eye symbol on Fig. 8, and characterizes the event as fast, or "snappy", i.e., with a spectrum blue-shifted towards higher frequencies, and hence producing larger accelerations and resulting in enhanced damage. Remarkably, all 13 values feature this behavior, and such redundancy further justifies the application of the algorithm to historical analog records. This behavior is in contrast to the 2015 Nepal and 2005 Pakistan earthquakes (Θ = −5.21 and − 4. 87, respectively) [Saloor and Okal, 2018].

Table 2
Summary of Θ results for 13 records.

Code	Component	Station	Distance (°)	Θ
NGS	*Z*	*Nagasaki, Japan*	*37.81*	*−4.44*
FKK	*Z*	*Fukuoka, Japan*	*38.19*	*−4.14*
HMD	*Z*	*Hamada, Japan*	*39.57*	*−4.38*
KOB	*Z*	*Kobe, Japan*	*42.13*	*−3.85*
OSK	*Z*	*Osaka, Japan*	*42.41*	*−4.25*
SHJ	*Z*	*Shiomisaki, Japan*	*42.69*	*−4.38*
NAG	*Z*	*Nagoya, Japan*	*43.56*	*−4.54*
OMA	*Z*	*Omaezaki, Japan*	*44.62*	*−3.92*
TOK	*Z*	*Tokyo, Japan*	*45.80*	*−4.44*
AKI	*Z*	*Akita, Japan*	*45.90*	*−4.16*
GTT	*Z*	*Göttingen, Germany*	*61.26*	*−4.28*
STR	*Z*	*Strasbourg, France*	*63.14*	*−4.28*
STR	*EW*	*Strasbourg, France*	*63.14*	*−4.29*

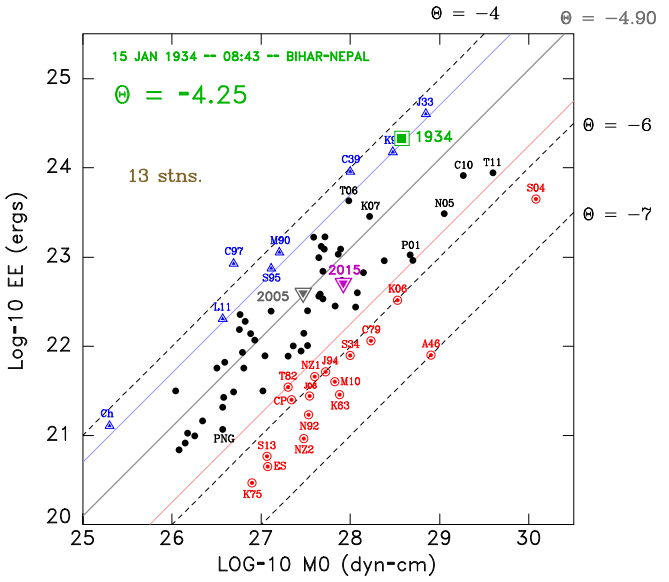

Fig. 8. Energy (ordinate) vs. Moment (abscissa) for a representative set of earthquakes [after Saloor and Okal, 2018]. Diagonal lines feature constant values of the slowness parameter Θ. The solid line in grey is the theoretical value under scaling laws (−4.90). The 1934 Bihar-Nepal earthquake is shown as the green square bull's eye symbol. Regular back- ground events are shown in black; those deficient in energy (Θ ≤ − 5. 80) shown in red include all so-called "tsunami earthquakes". Conversely fast, "snappy" earthquakes are shown as blue triangles (Θ ≥ − 4. 3). For reference, inverted triangles show the more regular earthquakes of 2015 in Nepal (magenta) and 2005 in Pakistan (grey). Labels identifying various events are listed in [Saloor and Okal, 2018]. (For interpretation of the references to colour in this figure legend, the reader is referred to the web version of this article.)

4. Implications

4.1. Implications for the regional seismic hazard assessment

This re-evaluation of the seismic moment released by the earthquake, more than 4 times greater than the lower values previously considered, has significant implications in term of regional seismic hazard assessment. In particular, it makes it possible to re-estimate the seismic moment deficit accumulated in eastern Nepal (Fig. 9).

Despite the uncertainties on the extent of the 1934 earthquake rupture, the field surveys conducted in the mesoseismal trace of the rupture (isoseismal VIII) revealed that geomorphological evidence points to a very young uplift corresponding either to surface rupture or localized subsurface ground deformation along a more than 143 km-long stretch of the Main Frontal Thrust, from at least Sir Khola near Bardibas to Sardu Khola near Dharan (Sapkota et al., 2013) (Figs. 1, 9

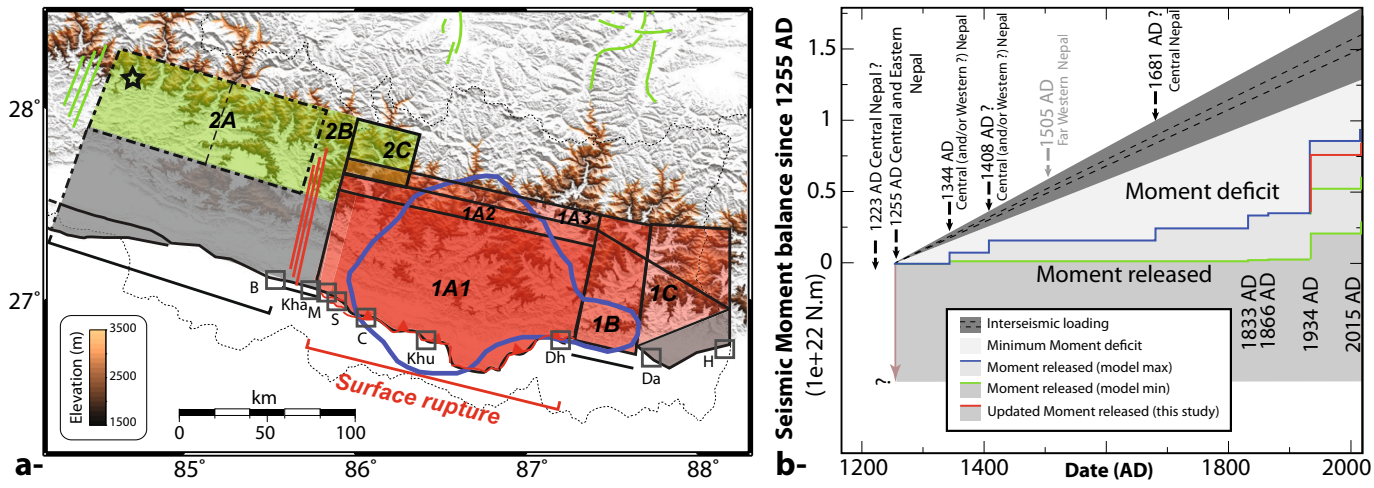

Fig. 9. (a): Rupture models for the 1833, 2015 and 1934 earthquakes, updated from Bollinger et al. (2016). Green patches 2A–2C correspond to segments of the Main Himalayan thrust having ruptured in 1833 and/or 2015. Red patches 1A-1B-1C correspond to various faults segments that eventually ruptured during the 1934 CE earthquake. B, Kh, M, S, C, Khu, Dh, Da and H, respectively, refer to the Bagmati, Khairmara, Mahara Khola, Sir Khola, Charnath, Khutti, Dharan, Damak and Hokse paleoseismological sites. (b): Accumulated moment deficit and co-seismic moment released due to major earthquakes from 1255 to 2015 along the 400-km-long eastern stretch of the Main Frontal Thrust, between the Kathmandu klippe and eastern India/Nepal border. Accumulated moment deficit rates and uncertainties (dark grey) are derived from the local seismic coupling model (Ader et al., 2012). Dashed lines show accumulation on a fully locked MHT over 80 km, assuming shortening rates of 18.5 and 17.5 mm/yr. Seismic moments released in 1833, 1866, and 2015 earthquakes are derived from published minimum (green) and maximum (blue) moment magnitude estimates for these events, the red line corresponds to the seismicity released by the 1934 earthquake as determined from this study. 1344 and 1408 CE earthquakes were assigned a moment release identical to the 1833 CE (green) and 2015 CE (blue) earthquakes. No post-seismic strain releases were taken into account in that budget, nor the duplex-related internal shortening estimated in Hu and Stevens (2022). (For interpretation of the references to colour in this figure legend, the reader is referred to the web version of this article.)

and 10).

The width of the fault rupture probably approaches the 70–80 km which corresponds to the total extent of the fully coupled upper segment of the MHT in eastern Nepal (Ader et al., 2012; Lindsey et al., 2018). This seems a reasonable hypothesis considering the minimum length of the rupture as well as the width of the mesoseismal area.

The Gorkha 2015 earthquake rupture was structurally controlled, abutting to the south at the toe of a ramp which develops below the Kathmandu klippe (Hubbard et al., 2016; Sathiakumar and Barbot, 2021). The rupture ended to the east of the trace of the Kathmandu klippe (e.g. Adhikari et al., 2015; Avouac et al., 2015; Bai et al., 2016; Yamada et al., 2020), a remnant of crystalline rocks covering the lesser Himalayas. Similarly, the rupture extent in 1934 was probably controlled by the geometry of the MHT at depth. We propose that the rupture abutted on a lateral ramp, suspected to develop to the East of the Kathmandu klippe (e.g. Letort et al., 2016; Baillard et al., 2017).

The length of the rupture in 1934, as debated in the literature (e.g., Pandey and Molnar, 1988; Molnar and Pandey, 1989; Bollinger et al., 2016; Bilham, 2019), is probably larger than the 143 km along which surface rupture was surveyed by Sapkota et al. (2013). The surface rupture necessarily stopped before the Bagmati river to the West, and before Damak to the East where the surface expression of the 1934 earthquake was not found – none of the sites having been ruptured since the 13th century according to the paleoseismological trenches excavated by Wesnousky et al. (2017a, 2017b).

This suggests that the surface rupture was smaller than the 185-km

Fig. 10. Photos of field outcrops illustrating well preserved surface expression of great surface rupturing earthquakes in the trace of the Bihar Nepal surface rupture and the associated challenges of determining lateral variations in coseismic slip (a- Top) The natural rivercut cliff of the Sir Khola affected by large folds and several thrust faults in the vicinity of the 30 m-high frontal cumulated scarp – the recent deformation is distributed through several structures-, (b- Bottom) poorly consolidated –30 m high- cumulated scarp on the east bank of Charnath Khola – the chaos of soft rocks is difficult to translate into incremental slip events before trenching.

length of the Main Frontal fault system that separate the two sites, provided that the rupture was not transferred to blind structures underneath the basins south of the MFT (e.g. Almeida et al., 2018; Duvall et al., 2020). The northward extension of the rupture likely corresponds to the downdip end of the locked fault zone, or to the brittle-ductile transition as mapped by Ader et al. (2012) or Lindsey et al. (2018). The distance between this area which develops at the toe of the high range and the surface trace of the fault measures approximately 70 to 90 km. Given a seismic moment of $M_0 = 3.8 \times 10^{28}$ dyn-cm (3.8×10^{21} N.m -$M_w = 8.3$), and assuming a crustal rigidity $\mu = 3 \times 10^{11}$ dyn/cm^2, we derive a seismic potency $P = M_0 / \mu$ of 1.27×10^{17} cm^3. The average slip on the fault then trades off with fault length and width as listed in Table 3.

The theoretical estimates of the coseismic slip we obtained from the evaluation of the seismic moment and from the extension of the rupture – between 7.9 and 15.1 m according to the model considered (Table 3)- have to be compared with the local subsurface slip estimated along the 1934 surface rupture. The coseismic slip is still poorly known along this surface rupture. Indeed, most of the scarps mapped along strike of the rupture are cumulated scarps built by several earthquakes (Fig. 10). Furthermore, several fault splays usually reach the surface while rare sedimentological markers are found offset by individual fault segments (the depositional environment being in general significantly different in the the foot and hanging walls of thrust faults). While incremental coseismic uplift of a horizontal terrace by faulting provides a measure of coseismic slip if the dip of the causal fault is known, and can be assumed to be planar, multiple faults can be activated making the determination of the total offset of a given earthquake particularly challenging when interpreting paleoseismic trenches.

At the Sir Khola, Charnath Khola and Khutti Khola paleoseismological sites (Fig. 9), we obtained the subsurface dip of the fault from seismic reflection imagery, or from structural mapping along the river-cut cliff (See Fig. 10 and Table 4). The resulting values of the coseismic slip feature large uncertainties, but fall within a range of 9 to 17 m for 1934 (Table 4 and Sapkota et al., 2013; Bollinger et al., 2014; Rizza et al., 2019; Riesner et al., 2023).

The estimates of the coseismic slip deduced from the seismic moment are therefore credible, reaching similar values. Note that a closer evaluation of the match between the model and sporadic field observations is risky, since the coseismic slip and its surface expression can be highly variable along the strike of a thrust fault (e.g. Philip et al., 1992; Boncio et al., 2018; Chiama et al., 2023). This variability has previously led to substantial underestimation of the magnitude of intracontinental thrust earthquakes based on morphotectonic evidence alone (e.g., Rubin, 1996).

However, to a first order, the slip transferred to the frontal thrust during the 1934 earthquake is consistent with the seismic slip deficit accumulated at a rate of ~18 mm/yr during the 679 years separating the penultimate great earthquake of 1255 and the Bihar–Nepal event of 1934 (Table 4).

4.2. Implications in a global context

In the previous sections, we obtained independent estimates of the seismic moment and the fault length of the 1934 Bihar-Nepal earthquake, $M_0 = 3.8 \times 10^{21}$ N.m ($M_w = 8.3$) and L = 145–175 km, respectively. This numbers are precious for any study of seismic risk from mega earthquakes along the Himalayan front, in particular regarding their recurrence, given the scarcity of such events over the era of instrumental seismology. It is then interesting to examine our results in the context of scaling laws describing the growth of source parameters (length L, width W, slip Δu; seismic moment M_0) with earthquake size. In very general terms, the presence of physical invariants in the processes governing earthquake rupture leads to the concept of these parameters growing in a related fashion with earthquake size, and eventually of a relationship between quantities such as L and M_0. Early attempts to explore such relations can be traced as far back as Tocher [1958], Press [1967] and Chinnery [1969], although they were hampered by the use of diverse magnitude scales. Landmark studies followed, including Kanamori and Anderson [1975] and Geller [1976], who proposed the relation.

$$M_0 = 1.45 \times 10^{20} \cdot L^3 \cdot \Delta\sigma \quad (4)$$

between seismic moment (in dyn-cm) and fault length (in km), with the stress drop Δσ in bars ranging between 30 and 50 bars for most large earthquakes. Assuming a stress droop Δσ = 35 bar, this is equivalent to.

$$\log_{10} L = 0.5\, M_w - 1.87 \quad (5)$$

Later catalogs such as Wells and Coppersmith [1994], and more recently Blaser et al. [2010], provided comparable relationships. Finally, and based on the constancy of energy-to-moment ratios extended to the study of laboratory microcracks, Ide and Beroza [2001] made the remarkable observation that the concept of seismic scaling laws could be applied across 17 orders of seismic moments. However, such studies generally used massive datasets of either regional events (e.g., in Southern California) or of mostly classical (i.e., oceanic) subduction earthquakes, We examine here the case of Himalayan events which could be intrinsically different, as they feature what amounts to continental subudction. For this purpose, we extracted from Blaser et al. [2010] database a subset of 80 events with $M_w \geq 5.2$ identified as "continental thrusts" (CT), and examined their fault lengths and moments (expressed as equivalent M_w), shown as blue dots on Fig. 11. Those CT events regress as.

$$\log_{10} L = 0.52\, M_w - 2.05 \text{ (CT)} \quad (6)$$

(green line on Fig. 10). We compare them to a set of 21 large oceanic thrust earthquakes (OT), shown as open squares. Those events regress as

$$\log_{10} L = 0.59\, M_w - 2.62 \text{ (OT)} \quad (7)$$

Finally, we also include on Fig. 11 Geller [1976] theoretical relation (5), computed for Δσ = 35 bar (blue dahsed line), as well as Wells and Coppersmith [1994] global regression.

$$\log_{10} L = 0.59\, M_w - 2.44 \quad (8)$$

Table 3
Seismic slip estimate for various hypotheses of rupture length and width illustrated on Fig. 9a.

Length (km)		140	160	180	200
Width (km)	60	15.1	13.2	11.8	10.6
	70	13.0	11.3	10.1	9.1
	80	11.3	9.9	8.8	7.9

Table 4
Seismic slip estimates of the Bihar Nepal earthquake at the principal sites where the surface rupture was studied.

Site Longitude/latitude (reference)	Minimum dip slip from local faults	Terrace elevation above river	Terrace derived slip estimates
Sir Khola 85.8720E/27.0482 N (Sapkota et al., 2013; Bollinger et al., 2014)	>3 m on F1, amount of slip on F3 and F4 unkown	+6 m for mad Buffalo channel	12–17.5 m (dip between 20° and 30°N)
Charnath 86.0824E/26.918 N (Rizza et al., 2019)	>3.3–8.5 m (from vertical offset and a dip of the fault @35–50°)	Offset PalT4 14 ± 3 m 15 m above T2	18–24.5 for 1934 or 1255 + 1934, 9–12 m for 1934
Khutti 86.4524E/26.798 N (Riesner et al., 2023)		Apparent vertical throw +8 m	~11–17 m with a thrust dipping between 30 and 45° N

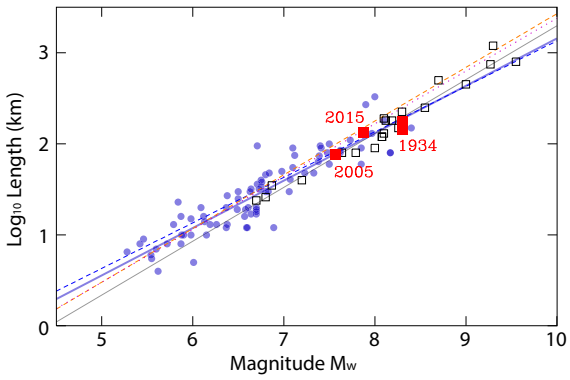

Fig. 11. Fault length L (logarithmic scale) vs. magnitude M_w for subsets of Blaser et al.'s (2010) dataset. Continental thrusts (CT) are shown as blue dots and regressed as the blue straight line (Eq. (6)), and large oceanic thrusts (OT) as open squares, regressed as the solid grey line (Eq. (7)). Also shown are Geller's (1976) theoretical relation (dark blue dashed line; Eq. (5)), and Wells and Coppersmith's (1994) global regression (orange dashed line; Eq. (8)) and reverse fault regression (magenta dotted line, Eq. (9)). Data for the 1934, 2015 and 2005 Himalayan earthquakes (Avouac et al., 2006) are shown as the large red squares; in the latter case, the symbol extends over the length axis to include the proposed range of estimates (145–175 km). (For interpretation of the references to colour in this figure legend, the reader is referred to the web version of this article.)

shown as the orange dashed line. We also include (magenta dotted line) their slightly different worldwide regression for reverse (thrust) faulting events.

$$\log_{10} L = 0.58\, M_w - 2.42 \quad (9)$$

Eqs. (6) and (7) predict fault lengths of 185 and 189 km, when applied to the moment magnitude of the 1934 Bihar earthquake, slightly overestimating the values reported above, but the latter remain within the scatter of the continental and oceanic thrust datasets on Fig. 11. This general agreement also applies to the 2015 Gorkha earthquake (slightly underestimated at 112 and 107 km, respectively) and to the 2005 Pakistan event (77 and 70 km). Geller [1976] theoretical relation (5) predicts very similar values (190 km for 1934, 118 km for 2015, and 82 km for 2005). By contrast, Wells and Coppersmith [1994] global relation (8) significantly overestimates fault lengths at 286 km (1934), 161 km (2015), and 106 km (2005), and so does their reverse faulting regression (9) with 247, 141 and 93 km, respectively. We conclude that the moment and fault length derived in this study for the 1934 Bihar-Nepal earthquake are in line with existing scaling laws, as obtained theoretically by Geller [1976] or empirically for continental thrust earthquakes, e.g., by Blaser et al. [2010], and that they can therefore be used legitimately, together with modern estimates for events such as the 2005 and 2015 earthquakes, in order to assess seismic risk from mega earthquakes along the Himalayan forefront.

5. Conclusions

With a seismic moment release of 3.8×10^{21} N.m, the Bihar Nepal earthquake was about 5 times larger than the 2015 earthquake. The rupture scenarii tested show that the average slip was probably between 8 and 16 m, a value significantly larger than deduced from previous estimates. This value is similar to the local estimates of coseismic slip at Sir Khola, Charnath Khola and Khutti Khola where it was estimated to be larger than 11 m. The amount of slip transposed to the front by the 1934 earthquake corresponds to first order with the seismic slip deficit accumulated (at 18 mm/yr) between the penultimate great earthquake that happened in 1255 and the Bihar Nepal event of 1934. In the above discussion, we have shown that independent observations such as field evidence and the location of the two main aftershocks can be used to infer properties such as fault length and mean seismic displacement. The general agreement under accepted scaling laws between these parameters and the seismic moment derived from mantle waves can be reconciled with the high value of the energy-to-moment parameter Θ if we assume a faster than usual rupture velocity. In the absence of digital data, it is however impossible to quantify this statement, and to venture a comparison with supershear rupture recently documented in a growing number of large strike-slip earthquakes and in the laboratory [e.g., Rosakis et al., 1999, 2025].

CRediT authorship contribution statement

Laurent Bollinger: Writing – original draft, Supervision, Methodology, Investigation, Formal analysis, Data curation, Conceptualization. **Emile A. Okal:** Writing – original draft, Methodology, Formal analysis, Data curation.

Declaration of competing interest

The authors declare that they have no known competing financial interests or personal relationships that could have appeared to influence the work reported in this paper.

Acknowledgments

We wish to express our gratitude to the colleagues and institutions who supported the works on the surface rupture of the Bihar Nepal earthquake, including the Department of Mines and Geology (Nepal), the CEA/DASE and IPGP (France) and the EOS (Singapore). This paper is written in memory of Paul Tapponnier, whose groundbreaking contributions to the study of active tectonics in general and to the study of the surface rupture of the 1934 earthquake have profoundly shaped this field. We thank Luis Rivera for providing copies of the Strasbourg seismograms. The authors sincerely thank Jochen Braunmiller and Roger Bilham for their thoughtful reviews, personal insights and valuable suggestions, which substantially strengthened this work. Some figures were prepared using the GMT software (Wessel and Smith, 1991).

Data availability

Data will be made available on request.

References

Abe, K., 1981. Magnitudes of large shallow earthquakes from 1904 to 1980. Phys. Earth Planet. Inter. 27 (1981), 72–92.
Abe, K., 1984. Complements to "Magnitudes of large shallow earthquakes from 1904 to 1980". Phys. Earth Planet. Inter. 34 (1984), 17–23.
Ader, T., Avouac, J.P., Liu-Zeng, J., Lyon-Caen, H., Bollinger, L., Galetzka, J., Genrich, J., Thomas, M., Chanard, K., Sapkota, S.N., Rajaure, S., Shrestha, P., Ding, L., Flouzat, M., 2012. Convergence rate across the Nepal Himalaya and interseismic coupling on the Main Himalayan Thrust: implications for seismic hazard. J. Geophys. Res. 117, B04403. https://doi.org/10.1029/2011JB009071.
Adhikari, L.B., Gautam, U.P., Koirala, B., Bhattarai, M., Kandel, T., Gupta, R.M., Timsina, C., Maharjan, N., Maharjan, K., Dahal, T., Hoste-Colomer, R., Cano, Y., Dandine, M., Guilhem, A., Merrer, S., Roudil, P., Bollinger, L., 2015. The aftershock sequence of the April 25 2015 Gorkha-Nepal earthquake. Geophys. J. Int. 203, 2119–2124.
Adhikari, L.B., Laporte, M., Bollinger, L., Vergne, J., Lambotte, S., Koirala, B.P., Bhattarai, M., Timsina, C., Gupta, R.M., Wendling-Vazquez, N., Batteux, D., Lyon-Caen, H., Gaudemer, Y., Bernard, P., Perrier, F., 2023. Seismically active structures of the Main Himalayan Thrust revealed before, during and after the 2015 Mw 7.9 Gorkha earthquake in Nepal. Geophys. J. Int. 232 (1), 451–471. https://doi.org/10.1093/gji/ggac281.
Almeida, R.V., Hubbard, J., Liberty, L., Foster, A., Sapkota, S.N., 2018. Seismic imaging of the Main Frontal Thrust in Nepal reveals a shallow décollement and blind thrusting. Earth Planet. Sci. Lett. 494, 216–225.
Ambraseys, N.N., Douglas, J., 2004. Magnitude calibration of north Indian earthquakes. Geophys. J. Int. 159, 165–206.
Avouac, J.P., Ayoub, F., Leprince, S., Konca, O., Helmberger, D.V., 2006. The 2005, Mw 7.6 Kashmir earthquake: sub-pixel correlation of ASTER images and seismic waveforms analysis. Earth Planet. Sci. Lett. 249 (3–4), 514–528.

Avouac, J.P., Meng, L., Wei, S., Wang, T., Ampuero, J.P., 2015. Lower edge of locked Main Himalayan Thrust unzipped by the 2015 Gorkha earthquake. Nat. Geosci. 8 (9), 708–711.
Bai, L., Liu, H., Ritsema, J., Mori, J., Zhang, T., Ishikawa, Y., Li, G., 2016. Faulting structure above the Main Himalayan Thrust as shown by relocated aftershocks of the 2015 Mw7. 8 Gorkha, Nepal, earthquake. Geophys. Res. Lett. 43 (2), 637–642.
Baillard, C., Lyon-Caen, H., Bollinger, L., Rietbrock, A., Letort, J., Adhikari, L.B., 2017. Automatic analysis of the Gorkha earthquake aftershock sequence: evidences of structurally segmented seismicity. Geophys. J. Int. 209 (2), 1111–1125.
Båth, M., Duda, S.J., 1979. Some aspects of global seismicity. In: Seismological Institute Reports. Uppsala Univ, pp. 1–79.
Ben-Menahem, A., 1961. Radiation of seismic surface waves from finite moving sources. Bull. Seismol. Soc. Am. 51, 401–435.
Bernard, O., et al., 2018. Evidence for repetitive 4 to 7m uplift of the MFT hangingwall in Suklaha Khola valley, Eastern Nepal. In: EGU Geophysical Research Abstracts, 20. EGU2018-17577.
Bijukchchen, S.M., Takai, N.Y., Shigefuji, M., Ichiyanagi, M., Sasatani, T., 2017. Estimation of 1-D velocity models beneath strong-motion observation sites in the Kathmandu Valley using strong-motion records from moderate-sized earthquakes. Earth Planets Space 69. https://doi.org/10.1186/s40623-017-0685-4.
Bilham, R., 1995. Location and magnitude of the 1833 Nepal earthquake and its relation to the rupture zones of contiguous great Himalayan earthquakes. Curr. Sci. 69 (2), 155–187.
Bilham, R., 2019. Himalayan earthquakes: a review of historical seismicity and early 21st century slip potential. Geol. Soc. Lond. Spec. Publ. 483 (1), 423–482.
Bilham, R., Blume, F., Bendick, R., Gaur, V.K., 1998. Geodetic constraints on the translation and deformation of India: implications for future great Himalayan earthquakes. Curr. Sci. 74 (3), 213–229.
Blaser, L., Krüger, F., Ohrnberger, M., Scherbaum, F., 2010. Scaling relations of earthquake source parameter estimates with special focus on subduction environment. Bull. Seismol. Soc. Am. 100 (6), 2914–2926.
Bollinger, L., Sapkota, S.N., Tapponnier, P., Klinger, Y., Rizza, M., Van der Woerd, J., Tiwari, D.R., Pandey, M.R., Bitri, A., Bes de Berc, S., 2014. Estimating the return times of great Himalayan earthquakes in Eastern Nepal: evidence from the Patu and Bardibas strands of the Main Frontal Thrust. J. Geophys. Res. https://doi.org/10.1002/2014JB010970.
Bollinger, L., Tapponnier, P., Sapkota, S.N., Klinger, Y., 2016. Slip deficit in Central Nepal: Omen for a repeat of the 1344AD earthquake? Earth Planets Space 68, 1–12. https://doi.org/10.1186/s40623-016-0389-1.
Bomford, G., 1937. Leveling in Bengal and Bihar. In: Couchman, H.J. (Ed.), Survey of India Geodetic Report 1936. Geodetic branch Survey of India, Dehra Dun, pp. 93–97.
Boncio, P., Liberi, F., Caldarella, M., Nurminen, F.C., 2018. Width of surface rupture zone for thrust earthquakes: implications for earthquake fault zoning. Nat. Hazards Earth Syst. Sci. 18 (1), 241–256.
Brice, A., Jayangondaperumal, R., Priyanka, R.S., Pandey, A., Mishra, R.L., Singh, I., Dash, S.P., 2024. Paleoseismological evidence for segmentation of the Main Himalayan Thrust in the Darjeeling-Sikkim Himalaya. Sci. Rep. 14 (1), 14537.
Brune, J.N., Engen, G.R., 1969. Excitation of mantle Love waves and definition of mantle wave magnitude. Bull. Seismol. Soc. Am. 59, 923–933.
Brune, J.N., King, C.Y., 1967. Excitation of mantle Rayleigh waves of period 100 s as a function of magnitude. Bull. Seismol. Soc. Am. 57, 1355–1365.
Chen, W.-P., Molnar, P., 1977. Seismic moments of major earthquakes and the average rate of slip in Central Asia. J. Geophys. Res. 82 (20), 2945–2969. https://doi.org/10.1029/JB082i020p02945.
Chiama, K., Chauvin, B., Plesch, A., Moss, R., Shaw, J.H., 2023. Geomechanical modeling of ground surface deformation associated with thrust and reverse-fault earthquakes: a distinct element approach. Bull. Seismol. Soc. Am. 113 (4), 1702–1723.
Chinnery, M.A., 1969. Earthquake magnitude and source parameters. Bull. Seismol. Soc. Am. 59, 1969–1982.
Dunn, J.A., Auden, J.B., Gosh, A.M.H., Roy, S.C., Wadia, D.N., 1939. The Bihar–Nepal earthquake of 1934. In: Memoirs of the Geological Survey of India, 73. Geological Survey of India.
Duvall, M.J., Waldron, J.W., Godin, L., Najman, Y., 2020. Active strike-slip faults and an outer frontal thrust in the Himalayan foreland basin. Proc. Natl. Acad. Sci. USA 117 (30), 17615–17621.
Dziewonski, A.M., Chou, T.-A., Woodhouse, J.H., 1981. Determination of earthquake source parameters from waveform data for studies of global and regional seismicity. J. Geophys. Res. 86, 2825–2852.
Ekström, G., Nettles, M., Dziewonski, A.M., 2012. The global CMT project 2004–2010: Centroid moment tensors for 13,017 earthquakes. Phys. Earth Planet. Inter. 200, 1–9.
Engdahl, E.R., van der Hilst, R., Buland, R.P., 1998. Global teleseismic earthquake relocation with improved travel times and procedures for depth relocation. Bull. Seismol. Soc. Am. 88, 722–743.
Geller, R.J., 1976. Scaling relations for earthquake source parameters and magnitudes. Bull. Seismol. Soc. Am. 66, 1501–1523.
Geller, R.J., Kanamori, H., 1977. Magnitudes of great shallow earthquakes from 1904 to 1952. Bull. Seismol. Soc. Am. 67, 587–598.
Grandin, R., Vallée, M., Satriano, C., Lacassin, R., Klinger, Y., Simoes, M., Bollinger, L., 2015. Rupture process of the Mw= 7.9 2015 Gorkha earthquake (Nepal): Insights into Himalayan megathrust segmentation. Geophys. Res. Lett. 42 (20), 8373–8382.
Gutenberg, B., Richter, C.F., 1941. Seismicity of the Earth. Geol. Soc. Am. Spec. Pap. 34, 125.
Gutenberg, B., Richter, C.F., 1949. Seismicity of the Earth and Associated Phenomena. Princeton Univ. Press, p. 273.
Gutenberg, B., Richter, C.F., 1954. Seismicity of the Earth and Associated Phenomena. Princeton Univ. Press, p. 310.
Gutenberg, B., Richter, C.F., 1956. Magnitude and energy of earthquakes. Ann. Geofis. 9, 1–15.
Hough, S.E., Bilham, R., 2008. Site response of the Ganges basin inferred from re-evaluated macroseismic observations from the 1897 Shillong, 1905 Kangra, and 1934 Nepal earthquakes. J. Earth Syst. Sci. 117 (S2), 773–782.
Hu, W.L., Stevens, V.L., 2022. Duplex kinematics reduces both frontal advance and seismic moment deficit in the Himalaya. Geology 50 (10), 1161–1165.
Hubbard, J., Almeida, R., Foster, A., Sapkota, S.N., Bürgi, P., Tapponnier, P., 2016. Structural segmentation controlled the 2015 Mw 7.8 Gorkha earthquake rupture in Nepal. Geology 44 (8), 639–642.
Ide, S., Beroza, G.C., 2001. Does apparent stress vary with earthquake size? Geophys. Res. Lett. 28, 3349–3352.
Kanamori, H., 1977. The energy release in great earthquakes. J. Geophys. Res. 82 (20), 2981–2987.
Kanamori, H., Anderson, D.L., 1975. Theoretical basis of some empirical relations in seismology. Bull. Seismol. Soc. Am. 65, 1073–1095.
Lavé, J., Yule, D., Sapkota, S.N., Basant, K., Madden, C., Attal, M., Pandey, M., 2005. Evidence for a great medieval earthquake (~1100 A.D.) in the Central Himalayas of Nepal. Science 307, 1302–1305.
Lee, W.H., Engdahl, E.R., 2015. Bibliographical search for reliable seismic moments of large earthquakes during 1900–1979 to compute MW in the ISC-GEM global instrumental reference earthquake catalogue. Phys. Earth Planet. Inter. 239, 25–32.
Letort, J., Bollinger, L., Lyon-Caen, H., Guilhem, A., Cano, Y., Baillard, C., Adhikari, L.B., 2016. Teleseismic depth estimation of the 2015 Gorkha-Nepal aftershocks. Geophys. J. Int. 207 (3), 1584–1595.
Lindsey, E.O., Almeida, R., Mallick, R., Hubbard, J., Bradley, K., Tsang, L.L., Hill, E.M., 2018. Structural control on downdip locking extent of the Himalayan megathrust. J. Geophys. Res. 123 (6), 5265–5278.
Marcussen, E., 2023. Acts of Aid: The Politics of Relief and Reconstruction after the 1934 Bihar-Nepal Earthquake. Cambridge University Press.
Martin, S., Szeliga, W., 2010. A catalog of felt intensity data for 570 earthquakes in India from 1636 to 2009. Bull. Seismol. Soc. Am. 100 (2), 562–569.
Molnar, P., Pandey, M.R., 1989. Rupture zones of great earthquakes in the Himalayan region. Proc. Indian Acad. Sci. (Earth Planet. Sci.) 98 (1), 61–70.
Molnar, P., Qidong, Deng, 1984. Faulting associated with large earthquakes and the average rate of deformation in central and eastern Asia. J. Geophys. Res. 89, 6203–6227. https://doi.org/10.1029/JB089iB07p06203.
Monsalve, G., Sheehan, A., Schulte-Pelkum, V., Rajaure, S., Pandey, M.R., Wu, F., 2006. Seismicity and one-dimensional velocity structure of the Himalayan collision zone: Earthquakes in the crust and upper mantle. J. Geophys. Res.: Solid Earth 111, B10301. https://doi.org/10.1029/2005JB004062.
Newman, A.V., Okal, E.A., 1998. Teleseismic estimates of radiated seismic energy: the E/M0 discriminant for tsunami earthquakes. J. Geophys. Res. 103, 26885–26898.
Okal, E.A., 2015. Historical seismograms: preserving an endangered species. GeoResJ 6, 53–64.
Okal, E.A., Borrero, J.C., 2011. The "tsunami earthquake" of 22 June 1932 in Manzanillo, Mexico: seismological study and tsunami simulations. Geophys. J. Int. 187, 1443–1459.
Okal, E.A., Kirby, S.H., 2002. Energy-to-moment ratios for damaging intraslab earthquakes: preliminary results on a few case studies. In: USGS Open File Rept., 02−328, pp. 127–131.
Okal, E.A., Talandier, J., 1989. Mm: a variable period mantle magnitude. J. Geophys. Res. 94, 4169–4193.
Okal, E.A., Kirby, S.H., Kalligeris, N., 2016. The Showa Sanriku earthquake of 1933 March 2: a global seismological reassessment. Geophys. J. Int. 206, 1492–1514.
Pandey, M.R., Molnar, P., 1988. The distribution of intensity of the Bihar-Nepal earthquake of 15 January 1934 and bounds on the extent of the rupture zone. J. Nepal Geol. Soc. 5 (1), 22–44.
Pant, M.R., 2002. A step toward a historical seismicity of Nepal. Adarsa 2, 29–60.
Philip, H., Rogozhin, E., Cisternas, A., Bousquet, J.C., Borisov, B., Karakhanian, A., 1992. The Armenian earthquake of 1988 December 7: faulting and folding, neotectonics and palaeoseismicity. Geophys. J. Int. 110 (1), 141–158.
Press, F., 1967. Dimensions of the source region for small shallow earthquakes. In: Proceedings of the VESIAC Conference on the Source Mechanism of Shallow Seismic Events, VESIAC Report 7885-1-x. Univ. Michigan, pp. 155–164.
Rana, B.S., 1935. Nepal Ko Maha Bhukampa (the Great Earthquake of Nepal). Jorganesh Press, Kathmandu, pp. 1–250 (in nepali).
Rees, B.A., Okal, E.A., 1987. The depth of the deepest historical earthquakes. Pure Appl. Geophys. 125, 699–715.
Richter, C.F., 1935. An instrumental earthquake magnitude scale. Bull. Seismol. Soc. Am. 25, 1–32.
Richter, C.F., 1958. Elementary Seismology. W.H. Freeman and Company, San Francisco, CA, p. 768.
Riesner, M., Bollinger, L., Rizza, M., Klinger, Y., Karakaş, Ç., Sapkota, S.N., Tapponnier, P., 2023. Surface rupture and landscape response in the middle of the great Mw 8.3 1934 earthquake mesoseismal area: Khutti Khola site. Sci. Rep. 13 (1), 4566.
Rizza, M., Bollinger, L., Sapkota, S.N., Tapponnier, P., Klinger, Y., Karakaş, C., Kali, E., Etchebes, M., Tiwari, D.R., Siwakoti, I., Bitri, A., Bes de Berc, S., 2019. Post-earthquake aggradation processes to hide surface ruptures in thrust systems: the M8.3, 1934, Bihar-Nepal earthquake ruptures at Charnath Khola (Eastern Nepal). J. Geophys. Res. https://doi.org/10.1029/2018JB016376.
Rosakis, A., Samudrala, O., Coker, D., 1999. Cracks faster than the shear wave speed. Science 284, 1337–1340.

Rosakis, A., Abdelmeguid, M., Elbanna, A., 2025. Near-field evidence for early supershear rupture of the Mw = 7. 8 Kahramanmaraş earthquake in Turkey. Nat. Geosci. 18, 534–541.
Roy, S.C., 1939. Seismometric study, chapter IV of 'the Bihar-Nepal earthquake of 1934'. In: Mem. Geol. Surv. India, pp. 49–75.
Rubin, C.M., 1996. Systematic underestimation of earthquake magnitudes from large intracontinental reverse faults: historical ruptures break across segment boundaries. Geology 24 (11), 989–992.
Salaree, A., Okal, E.A., 2018. The "tsunami earthquake" of 13 April 1923 in Northern Kamchatka: seismological and hydrodynamic investigations. Pure Appl. Geophys. 175, 1257–1285.
Saloor, N., Okal, E.A., 2018. Extension of the energy-to-moment parameter Θ to intermediate and deep earthquakes. Phys. Earth Planet. Inter. 274, 37–48.
Saloor, N., Okal, E.A., 2020. The body-wave magnitude mb: an attempt to rationalize the depth distance correction q(Δ, h). Geophys. J. Int. 223, 270–288.
Sapkota, S.N., 2011. Surface Rupture of 1934 Bihar-Nepal Earthquake: Implications for Seismic Hazard in Nepal Himalaya. Unpublished thesis. IPGP, pp. 1–292.
Sapkota, S.N., Bollinger, L., Klinger, Y., Tapponnier, P., Gaudemer, Y., Tiwari, D.R., 2013. Primary surface rupture of the great Himalayan earthquakes of 1934 and 1255. Nat. Geosci. 6, 71–76. https://doi.org/10.1038/ngeo1669.
Sapkota, S.N., Bollinger, L., Perrier, F., 2016. Fatality rates of the Mw~ 8.2, 1934, Bihar–Nepal earthquake and comparison with the April 2015 Gorkha earthquake. Earth Planets Space 68 (1), 1–9.
Sathiakumar, S., Barbot, S., 2021. The stop-start control of seismicity by fault bends along the Main Himalayan Thrust. Commun. Earth Environ. 2 (1), 87.
Singh, D.D., Gupta, H.K., 1980. Source dynamics of two great earthquakes of the Indian subcontinent: the Bihar-Nepal earthquake of January 15, 1934 and the Quetta earthquake of May 30, 1935. Bull. Seismol. Soc. Am. 70, 757–773.
Stevens, V.L., Avouac, J.P., 2016. Millenary Mw> 9.0 earthquakes required by geodetic strain in the Himalaya. Geophys. Res. Lett. 43 (3), 1118–1123.
Subedi, S., Hetényi, G., 2021. Precise locating of the great 1897 Shillong Plateau Earthquake using teleseismic and regional seismic phase data. Seism. Rec. 1 (3), 135–144.
Szeliga, W., Hough, S., Martin, S., Bilham, R., 2010. Intensity, magnitude, location, and attenuation in India for felt earthquakes since 1762. Bull. Seismol. Soc. Am. 100 (2), 570–584.
Tocher, D., 1958. Earthquake energy and ground breakage. Bull. Seismol. Soc. Am. 48, 147–153.
Tsai, V.C., Hayes, G.P., Duputel, Z., 2011. Constraints on the long-period moment-dip trade-off for the Tohoku earthquake. Geophys. Res. Lett. 38 (7), L00G17.
Vaněk, J., Zátopek, A., Kárnıák, V., Kondorskaya, N.V., Riznichenko, Yu.V., Savarensky, E.F., Solov'ev, S.L., Shebalin, N.V., 1962. Standardization of magnitude scales. Bull. Acad. Sci. USSR Geophys. Ser. 2, 108–111.
Wang, K., Fialko, Y., 2015. Slip model of the 2015 Mw = 7. 8 Gorkha (Nepal) earthquake from inversions of ALOS-2 and GPS data. Geophys. Res. Lett. 42, 7452–7458.
Wells, D.L., Coppersmith, K.J., 1994. New empirical relationships among magnitude, rupture length, rupture width, rupture area, and surface displacement. Bull. Seismol. Soc. Am. 84, 974–1002.
Wesnousky, S.G., Kumahara, Y., Chamlagain, D., Pierce, I.K., Karki, A., Gautam, D., 2017a. Geological observations on large earthquakes along the Himalayan frontal fault near Kathmandu, Nepal. Earth Planet. Sci. Lett. 457, 366–375.
Wesnousky, S.G., Kumahara, Y., Chamlagain, D., Pierce, I.K., Reedy, T., Angster, S.J., Giri, B., 2017b. Large paleoearthquake timing and displacement near Damak in eastern Nepal on the Himalayan Frontal Thrust. Geophys. Res. Lett. 44 (16), 8219–8226.
Wesnousky, S.G., Kumahara, Y., Chamlagain, D., Neupane, P.C., 2019. Large himalayan frontal thrust paleoearthquake at Khayarmara in Eastern Nepal. J. Asian Earth Sci. 174, 346–351.
Wessel, P., Smith, W.H.F., 1991. Free software helps map and display data. EOS Trans. Am. Geophys. Union 72 (441), 445–446.
Wysession, M.E., Okal, E.A., Miller, K.L., 1991. Intraplate seismicity of the Pacific Basin, 1913–1988. Pure Appl. Geophys. 135, 261–359.
Yamada, M., Kandel, T., Tamaribuchi, K., Ghosh, A., 2020. 3D fault structure inferred from a refined aftershock catalog for the 2015 Gorkha earthquake in Nepal. Bull. Seismol. Soc. Am. 110 (1), 26–37.